VEIN SEGMENTATION USING SHAPE-BASED MARKOV RANDOM FIELDS

Phillip G. D. Ward[1, 2] Nicholas J. Ferris[1, 3] Parnesh Raniga[1, 4]
Amanda C. L. Ng[5] David G. Barnes[2, 6] David L. Dowe[2] Gary F. Egan[1, 7]

[1]Monash Biomedical Imaging, Monash University, Clayton VIC, Australia.
[2]Faculty of Information Technology, Monash University, Clayton VIC, Australia.
[3]Monash Imaging, Monash Health, Clayton VIC, Australia.
[4]The Australian eHealth Research Centre, CSIRO Health and Biosecurity, Herston QLD, Australia.
[5]Department of Anatomy and Neuroscience, The University of Melbourne, Melbourne VIC, Australia.
[6]Monash Immersive Visualisation Platform, Monash University, Clayton VIC, Australia.
[7]ARC Centre of Excellence for Integrative Brain Function, Melbourne VIC, Australia.

ABSTRACT

The magnetic susceptibility of haemoglobin is modulated by oxygen saturation, providing a mechanism to non-invasively measure oxygen extraction fraction. When combined with perfusion techniques, quantitative susceptibility mapping facilitates regional measurement of cerebral metabolic rate of oxygen consumption. However, accurate measurement requires a complete vein map to measure anatomical variance in the metabolic demands of tissue. In this work we present a novel shape-based Markov Random Field technique to segmentation the cerebral veins that provides accurate and complete vein maps. The shape-based graph underpinning the model controls the spatial relationships between voxels and enforces cylindrical geometry, allowing increased sensitivity with accurate vein boundaries.

Index Terms— vein segmentation, quantitative susceptibility mapping, oxygen extraction fraction

1. INTRODUCTION

Venous pathophysiology has been associated with multiple-sclerosis, dementia and healthy ageing [1]–[3], and correlations have been observed between the venous vasculature and biomarkers of small vessel disease [4]. Studies of these processes in large healthy populations require minimally invasive, and automated, methods of quantifying cerebral metabolism and vascular health.

Quantitative susceptibility mapping (QSM) is a new technique to measure magnetic susceptibility differences within the brain [5], [6], and has been used to measure venous oxygen saturation (S_VO_2) in vivo [3], [7]. In combination with MRI-based perfusion, MRI-based S_VO_2 can be used to derive the cerebral metabolic rate of oxygen consumption ($CMRO_2$) [7] without invasive contrast agents.

$CMRO_2$ is a tissue-based measure and requires a map of tissue oxygen extraction fraction (OEF) measuring the difference in arterial and venous oxygen saturation. Thus, S_VO_2 must be extrapolated from veins to the nearby tissue. To capture anatomical S_VO_2 variation, and correctly map tissue to veins, complete vein maps are essential. Unfortunately though, large downstream veins contain blood drained from multiple regions and lack anatomical specificity, and conversely, small veins are difficult to identify and can suffer partial volume effects.

Metabolic impairment in the frontal and parietal regions has been identified in dementia and is a potential biomarker of cognitive compensation [8]. Fortunately, the pial veins in these regions are well suited to $CMRO_2$ measurements due to their size, contrast and anatomical coverage. In other regions, such as the temporal lobe and subcortical structures, vein contrast is reduced due to susceptibility artifacts and iron accumulation in the tissue.

Numerous methods have been proposed for MRI-based vein segmentation [9]–[11]. Shape-driven diffusion and graph-based approaches have been proposed to enhance continuity and preserve narrow structures [9], [10]. When increasing the sensitivity of these methods, graph-based approaches often lack specificity due to the indiscriminant nature of their sensitivity terms. Diffusion approaches are more constrained, particularly shape-driven diffusion [9], however they may be too rigid for vessels of high curvature and insensitive to small vessels with low contrast.

In this work a shape-based Markov Random Field technique (ShMRF) is proposed for vein segmentation and evaluated on frontal and parietal pial veins. ShMRF combines the statistical graph-based approaches with shape-driven spatial dependencies. To our knowledge this direct coupling of spatial dependencies and shape information is novel, and allows for scale- and orientation-specific neighborhood profiles that focus graph sensitivity along vein centerlines, preserving narrow veins without exaggerating the boundaries of large veins. Veins were segmented from the QSM images using ShMRF and two alternative techniques from the literature, and compared with manually traced ground-truth. Accuracy was assessed using traditional overlap measures and differences in tissue-

based OEF maps in the parietal and frontal regions generated from the vein segmentations.

2. METHODS

The purpose of a vein segmentation algorithm is to take an input image and produce a vein map, $\alpha(r)$, where $\alpha(r) = 1$ for vein voxels, and $\alpha(r) = 0$ for non-vein voxels (estimates are denoted with primes, e.g., $\alpha'(r)$).

2.1 Markov Random Field

The MRF was derived from the Ising model [12]. It had two energy terms namely a data term and a smoothness term ($E(r) = E_D(r) + E_S(r)$), with labels chosen to minimize the total energy. A two-component (vein, non-vein) Gaussian Mixture Model (GMM) was fitted to the QSM image using expectation maximization [13]. The mixing proportions, $m_v(r)$ and $m_{nv}(r)$, were used in the data term.

$$E_D(r) = \begin{cases} \log\big(m_v(r)\big), & \alpha'(r) = 1 \\ \log\big(m_{nv}(r)\big), & \alpha'(r) = 0 \end{cases} \quad (1)$$

The smoothness term penalizes higher numbers of voxels with opposing labels in the voxels' neighborhood or clique (ζ), multiplied by a graph weight ($\omega(r,i)$), where i denotes the i[th] voxel in the clique of r.

$$E_S(r) = \sum_{i \in \zeta} \omega(r,i) \cdot |\alpha'(r) - \alpha'(r_i)| \quad (2)$$

In an isotropic graph, $\omega(r,i) = \omega_0$. In [10] a label-specific anisotropic graph was employed to account for the uneven ratio of non-vein neighbors to long-thin veins.

$$\omega(r,i) = \begin{cases} \omega_1, & \alpha'(i) = 1 \\ \omega_2, & \alpha'(i) = 0 \end{cases} \quad (3)$$

2.2 Shape-based Graph

One of the most commonly used vessel enhancement filters is the Hessian-based vesselness filter [11], which uses the eigenvalues of the Hessian matrix in a vessel response function. In ShMRF, the graph was weighted by agreement between neighbor direction and the estimated vein centerline ($U'(r)$), represented by the eigenvector of the smallest eigenvalue of the Hessian matrix.

$$\omega(r,i) = \frac{|N|}{\sum_i^{\zeta} \Omega(r,i)} \cdot \begin{cases} \omega_1 \cdot \Omega(r,i), & \alpha'(i) = 1 \\ \omega_2 \cdot \Omega(r,i), & \alpha'(i) = 0 \end{cases} \quad (4)$$

$$\Omega(r,i) = |\theta(r,i) \cdot U'(r)|^2 \quad (5)$$

where $\theta(r,i)$ is the unit vector from r to the i[th] voxel in ζ, and N is the size of the neighborhood (3x3x3). The vein neighbors are not evenly influenced (Eq. 4); rather the influence is focused on voxels in the direction of a proposed vein centerline ($U'(r)$). The weights were normalized, to ensure a unity mean weight. The final model was optimized using iterative conditional modes.

2.3 Oxygen extraction fraction (OEF) mapping

OEF was estimated using the vein susceptibility (χ_{vein}) relative to ventricular CSF (χ_{ref}).

$$\mathrm{OEF}(r) = \big(\chi_{vein} - \chi_{ref}\big)/(\chi_{do} \cdot Hct) \quad (6)$$

where χ_{do} is fully-deoxygenated haemoglobin ($4\pi \times 0.27$ ppm) and Hct is haematocrit (0.4) [3]. A nearest-neighbor approach was taken to assigning venous measurements to tissue. To reduce partial volume effects, maximum filtering was performed along connected components of a temporarily dilated vein map. Maximum filtering replaced each vein map voxel with the maximum intensity vein map voxel within a 10-voxel distance along a connected path.

3. EXPERIMENTS

3.1. Acquisition

Four healthy volunteers (3 female, mean age 26.0 years, standard deviation 5.4 years) were scanned on a 3T Siemens Skyra with a 32-channel head-neck coil using a single echo, flow-compensated, gradient-recalled echo (GRE) sequence (TE=20ms, TR=30ms, voxel=0.9x0.9x0.9mm, matrix=256×232×160, flip angle=15^o).

3.2. Data processing

Raw k-space data was saved for each channel for phase and magnitude image reconstruction. Individual coil phase images were processed to remove phase wraps and background phase using Laplacian unwrapping [14] and V-SHARP processing [15]. QSM maps were computed using LSQR in the STI-Suite [14]. SWI images were also processed and taken directly from the scanner console. Parietal and frontal regions were identified using an atlas [19] and linearly registered from MNI space to subject space based upon the GRE magnitude using FLIRT [16], [17].

3.3. Vein delineation

Veins were manually traced by one of the authors (PW) under the supervision of a clinical radiologist (NF) using both SWI and QSM. Where QSM and SWI disagreed, knowledge of anatomy and expert judgment was used. An example slice taken is shown in Fig. 1. The inclusion of SWI in this process increased sensitivity to smaller veins.

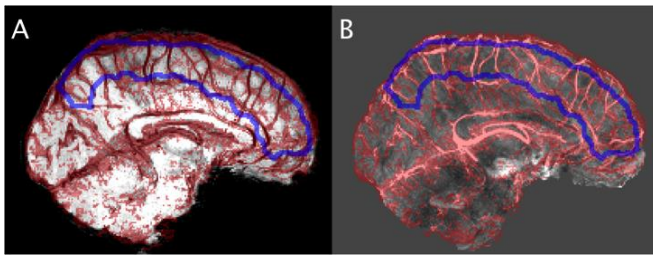

Fig. 1. Intensity projections (9mm) for SWI (minimum) (A) and QSM (maximum) (B), with vein ground-truth overlay in red and fronto-parietal region outlined in blue.

3.4. Comparison

For comparison, the vesselness filter (VN, [11]), and a recursive-ridged based filter (RR, [9]) were examined. Recommended parameter values were used for RR. VN and ShMRF parameters were tuned using a leave-one-out method, i.e., the parameters for subject x were trained on $y \in S/\{x\}$. A gridded search (1% of parameter space grid) was performed for each training instance. Performance was assessed using mean Hausdorff distance (MHD, [18]) minus the dilated Dice-Sorenson similarity measure (DSS, [9]).

$$MHD = \left(\mathfrak{D}(\alpha, \alpha') + \mathfrak{D}(\alpha', \alpha)\right)/2 \quad (7)$$

where $\mathfrak{D}(A, B)$ is the mean distance of all surface voxels in A to the nearest voxel in B. Surface voxels were those removed by morphological erosion (3x3x3 kernel). Average volume difference ($AVD = |FP - FN|/TP + FN$) was also used to compare the techniques.

4. RESULTS

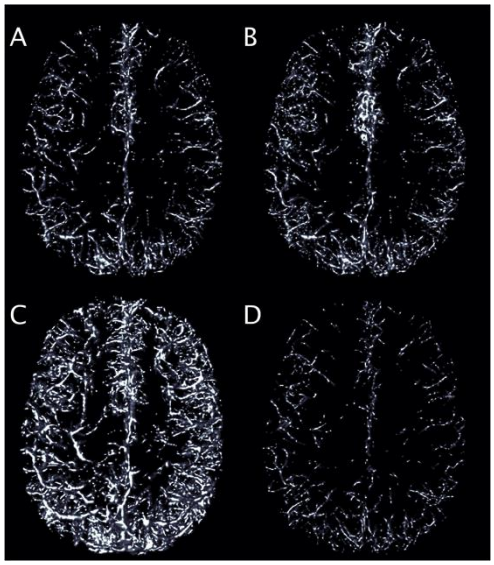

Fig. 2. 2D-Projections of cortical region in axial view for (A) ground truth, (B) ShMRF, (C) VN and (D) RR. The projection was of semi-transparent layers, as such, vessel volume influences pixel intensity (brighter equals larger).

The projections shown in Fig. 2 visualise the density of the three techniques. ShMRF technique has increased continuity in smaller veins in comparison to RR. The VN technique was highly sensitive, generating many false positives. ShMRF recorded superior performance to the VN and RR techniques in the five of the six comparisons (Table 1).

Table 1. Scores in combined frontal and parietal regions.

	Ideal	ShMRF	VN	RR
MHD	0	1.21±0.13	1.46 ±0.11	1.68 ±0.27
DSS	1	0.61±0.04	0.53±0.04	0.38±0.06
AVD	0	0.53±0.05	0.52±0.05	0.86±0.03

OEF maps were calculated using ground-truth vein maps, and maps from the three automatic methods. Automated maps minus ground-truth maps are shown in Fig. 3B-D. The ShMRF vein map had the lowest residuals (Fig. 3B) compared to the VN and RR vein maps (Fig. 3C and D). The ShMRF and VN technique had a negative bias, and RR technique had a positive bias.

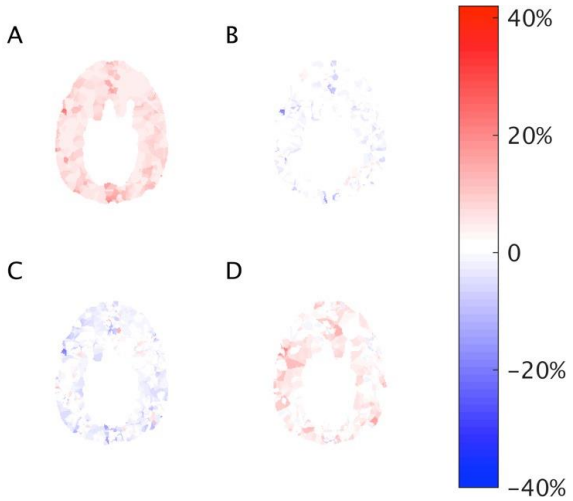

Fig. 3. (A) Axial slice from tissue OEF map calculated using the ground-truth manually traced vein map. Difference images for (B) ShMRF, (C) VN and (D) RR minus (A).

ShMRF was found to have lower root mean-squared error (RMSE) in OEF maps compared to VN and RR techniques (Wilcoxon rank-sum test, $p \cong 0.03$ for both) (Table 2). The ShMRF approach required less than 5 minutes per subject on a desktop machine, and was comparable to VN and RR.

Table 2. RMSE in OEF maps in combined frontal and parietal regions relative to manual tracing.

ShMRF	VN	RR
2.9%±0.4%	4.4%±0.3%	4.3%±0.4%

5. DISCUSSION AND CONCLUSIONS

Advances in QSM have enabled non-invasive local measurement of $CMRO_2$, however complete venograms are necessary to capture variation in tissue OEF. Tissue with few or no segmented veins nearby must be assigned to more distant vessels, and is unlikely to be accurately measured (as was depicted in Fig 3D). In such a scenario, large homogenous regions on the OEF map grow.

The shape-based Markov Random Field technique provided the most complete and accurate vein maps of the three segmentation techniques examined. The ShMRF technique achieved higher specificity than VN, whilst maintaining higher sensitivity than RR, by predicating shape-based influence on neighborhood labels. The framework ensures shape-enhancement only originates from

voxels that are labeled vein. Without this constraint, distinct objects may be joined together, as the VN is prone to do. Whilst the RR technique did not score as highly on the examined metrics, due primarily to reduced sensitivity, the specificity was comparable for this technique and ShMRF.

Future work could include comparing with other vascular segmentation methods (e.g. [19]).

OEF difference images showed a negative bias for ShMRF, which is indicative of false-positives or segmenting small veins that are adversely affected by partial volume. Visual inspection of the ShMRF venograms suggests the latter. Maximum filtering cannot mitigate partial volume when pure vein voxels are sparse, as is expected for small veins. Future work will address the effect of partial volume.

6. ACKNOWLEDGEMENTS

We thank all of subjects for their time and willingness to participate, and the radiologists and technical staff who acquired the images. The Alzheimer's Australia Dementia Research Foundation (AADRF), the Victorian Life Sciences Computation Initiative (VLSCI), and the Multi-model Australian ScienceS Imaging and Visualisation Environment (MASSIVE) supported this work.

7. REFERENCES

[1] W. R. Brown and C. R. Thore, "Review: Cerebral microvascular pathology in aging and neurodegeneration," *Neuropathol. Appl. Neurobiol.*, vol. 37, no. 1, pp. 56–74, 02 2011.

[2] M. I. Gaitán, M. P. de Alwis, P. Sati, G. Nair, and D. S. Reich, "Multiple sclerosis shrinks intralesional, and enlarges extralesional, brain parenchymal veins," *Neurology*, vol. 80, no. 2, pp. 145–151, 01/08 2013.

[3] A. P. Fan *et al.*, "Quantitative oxygen extraction fraction from 7-Tesla MRI phase: reproducibility and application in multiple sclerosis," *J. Cereb. Blood Flow Metab.*, vol. 35, no. 1, pp. 131–139, Jan. 2015.

[4] Y. Ge *et al.*, "Dynamic Susceptibility Contrast Perfusion MR Imaging of Multiple Sclerosis Lesions: Characterizing Hemodynamic Impairment and Inflammatory Activity," *AJNR Am J Neuroradiol*, vol. 26, no. 6, pp. 1539–1547, 2005.

[5] J. P. Marques and R. Bowtell, "Application of a Fourier-based method for rapid calculation of field inhomogeneity due to spatial variation of magnetic susceptibility," *Concepts Magn. Reson. Part B Magn. Reson. Eng.*, vol. 25B, no. 1, pp. 65–78, 2005.

[6] R. Salomir, B. D. de Senneville, and C. T. Moonen, "A fast calculation method for magnetic field inhomogeneity due to an arbitrary distribution of bulk susceptibility," *Concepts Magn. Reson. Part B Magn. Reson. Eng.*, vol. 19B, no. 1, pp. 26–34, 2003.

[7] J. Zhang, T. Liu, A. Gupta, P. Spincemaille, T. D. Nguyen, and Y. Wang, "Quantitative mapping of cerebral metabolic rate of oxygen (CMRO2) using quantitative susceptibility mapping (QSM)," *Magn. Reson. Med.*, vol. 74, no. 4, pp. 945–952, Oct. 2015.

[8] S. L. Risacher and A. J. Saykin, "Neuroimaging Biomarkers of Neurodegenerative Diseases and Dementia," *Semin. Neurol.*, vol. 33, no. 4, pp. 386–416, Sep. 2013.

[9] P. L. Bazin, V. Plessis, A. P. Fan, A. Villringer, and C. J. Gauthier, "Vessel segmentation from quantitative susceptibility maps for local oxygenation venography," in *2016 IEEE 13th International Symposium on Biomedical Imaging (ISBI)*, 2016, pp. 1135–1138.

[10] S. Bériault, M. Archambault-Wallenburg, A. Sadikot, D. Louis Collins, and G. Bruce Pike, "Automatic Markov Random Field Segmentation of Susceptibility-Weighted MR Venography," in *Clinical Image-Based Procedures. Translational Research in Medical Imaging*, 2014, pp. 39–47.

[11] A. F. Frangi, W. J. Niessen, K. L. Vincken, and M. A. Viergever, "Multiscale vessel enhancement filtering," in *Medical Image Computing and Computer-Assisted Intervention — MICCAI'98*, W. M. Wells, A. Colchester, and S. Delp, Eds. Springer Berlin Heidelberg, 1998, pp. 130–137.

[12] R. C. Dubes and A. K. Jain, "Random field models in image analysis," *J. Appl. Stat.*, vol. 16, no. 2, pp. 131–164, 1989.

[13] A. P. Dempster, N. M. Laird, and D. B. Rubin, "Maximum Likelihood from Incomplete Data via the EM Algorithm," *J. R. Stat. Soc. Ser. B Methodol.*, vol. 39, no. 1, pp. 1–38, Jan. 1977.

[14] W. Li, A. V. Avram, B. Wu, X. Xiao, and C. Liu, "Integrated Laplacian-based phase unwrapping and background phase removal for quantitative susceptibility mapping," *NMR Biomed.*, vol. 27, no. 2, pp. 219–227, Feb. 2014.

[15] F. Schweser, A. Deistung, B. W. Lehr, and J. R. Reichenbach, "Quantitative imaging of intrinsic magnetic tissue properties using MRI signal phase: An approach to in vivo brain iron metabolism?," *NeuroImage*, vol. 54, no. 4, pp. 2789–2807, Feb. 2011.

[16] J. Mazziotta *et al.*, "A probabilistic atlas and reference system for the human brain: International Consortium for Brain Mapping (ICBM).," *Philos. Trans. R. Soc. Lond. Ser. B*, vol. 356, no. 1412, pp. 1293–1322, Aug. 2001.

[17] M. Jenkinson, C. F. Beckmann, T. E. J. Behrens, M. W. Woolrich, and S. M. Smith, "FSL," *NeuroImage*, vol. 62, no. 2, pp. 782–790, Aug. 2012.

[18] R. Shonkwiler, "An image algorithm for computing the Hausdorff distance efficiently in linear time," *Inf. Process. Lett.*, vol. 30, no. 2, pp. 87–89, Jan. 1989.

[19] M. W. K. Law and A. C. S. Chung, "An Oriented Flux Symmetry Based Active Contour Model for Three Dimensional Vessel Segmentation," in *Computer Vision – ECCV 2010*, 2010, pp. 720–734.